

Early galaxy evolution from deep wide field star counts

I. The spheroid density law and mass function

A.C. Robin¹, C. Reylé¹, and M. Crézé²

¹ CNRS ESA6091, Observatoire de Besançon, B.P. 1615, 25010 Besançon Cedex, France (annie.robin,celine.reyle@obs-besancon.fr)

² Université de Bretagne-Sud, 56000 Vannes, France (michel.creze@univ-ubs.fr)

Received 9 March 2000 / Accepted 27 March 2000

Abstract. As part of a global analysis of deep star counts to constrain scenarios of galaxy formation and evolution, we investigate possible links between the galactic spheroid and the dark matter halo. A wide set of deep star counts at high and intermediate galactic latitudes is used to determine the large scale density law of the spheroid. Assuming a power density law, the exponent, flattening, local density and IMF slope of this population are estimated. The estimation is checked for robustness against contamination of star counts by the thick disc population. Contamination effects are derived from a model of population synthesis under a broad variety of thick disc parameters. The parameter fit is based on a maximum likelihood criterion. The best fit spheroid density law has a flattening of 0.76, a power index of 2.44. There is a significant degeneracy between these two parameters. The data are also compatible with a slightly less flattened spheroid ($c/a = 0.85$), in combination with a larger power index (2.75). A flatter spheroid ($c/a = 0.6$) with a power index of 2 is not excluded either. We also constrain the spheroid IMF slope α to be 1.9 ± 0.2 , leading to a local density of $1.64 \cdot 10^{-4}$ stars pc^{-3} and a mass density of $4.15 \cdot 10^{-5} M_{\odot} \text{pc}^{-3}$. With this slope the expected mass density of brown dwarfs in the halo makes a negligible part of the dark matter halo, as already estimated from microlensing surveys.

So, as star count data progresses in depth and extent, the picture of the spheroid star population that comes out points to a shape quite compatible with what we know about the distribution of baryonic dark matter if it is made of stellar remnants, suggesting a common dynamical origin.

Key words: Galaxy: halo – Galaxy: formation – Galaxy: stellar content – cosmology: dark matter – Galaxy: general

1. Introduction

This paper is part of a global analysis of star counts developed to constrain consistently scenarios of galaxy formation and evolution. The central tool of this approach is the “Besançon” model of population synthesis. This model is gradually tuned to fit an increasing number of observational constraints while

keeping compatibility with previous fits and theoretical prescriptions. In the present paper we address the problem of the halo (dark or visible) by trying to compare the properties of the spheroid population (the visible halo) with the dark matter halo, as traced by microlensing at high galactic latitudes and by the rotation curve. If the dark matter is made at least partly of stellar remnants, as shown by recent statistics of microlensing at high galactic latitudes (Aubourg et al., 1993; Alcock et al., 1997; Alcock et al., 1998), the density trend of this matter should be close to a power law with index of 2 (as expected from a flat rotation curve). It is natural to think of a similar shape for the stellar spheroid.

Constraints on the overall shape of the dark halo are poor. Cosmological simulations of halo formation generally predict that halos are flattened by about $c/a \sim 0.7$ (Rix, 1996). But the axis ratio depends on how much the halo matter is dissipative, the more dissipative, the flatter the halo. Direct determinations of the dark matter distribution in polar ring galaxies show flattened halos with $c/a \sim 0.5$ (Sackett et al., 1994; Rix, 1996).

Concerning the spheroid population, most previous analyses suggest rather steep density slopes with power indices between 3.0 and 3.5. However, these analyses are based on rather small samples of well identified tracers. The estimated flattening also cover a wide range between 0.6 to 1.0:

The distribution of galactic globular clusters appears to be well fitted by a power law density with index $n \sim 3.5$ and flattening of 1 (Harris, 1976; Zinn, 1985). Hawkins RR Lyrae observations (1984) showed $n = 3.1 \pm 0.2$ with a flattening of 0.9. Saha (1985), using a spherically symmetric model, found $n \sim 3$ out to 25 kpc but then the RR Lyrae density falls off more rapidly beyond 25 kpc. Another study of RR Lyrae by Wetterer (1996) showed that a spherically symmetric model yields $n \sim 3$ whereas an ellipsoidal distribution yields $n \sim 3.5$. Sluis (1998) counted blue horizontal branch (BHB) stars and RR Lyrae and found $c/a \sim 0.5$ and $n = 3.2 \pm 0.3$. Still from BHB star counts, Sommer-Larsen (1987) derived $c/a \sim 0.8$ and $n \sim 3$ up to 40 kpc, Preston (1991) found that c/a increases from 0.5 to 1 up to 20 kpc with $n = 3.5$. Soubiran (1993) showed that $n = 3.5 \pm 0.5$ is compatible with the kinematical behavior of a star sample near the north galactic pole. K dwarf counts with HST yield $c/a = 0.8 \pm 0.1$ and $n = 3.06 \pm 0.22$ (Gould et al., 1998). All of these studies were based on a few hundred objects at most.

Send offprint requests to: A.C. Robin

Correspondence to: Annie.Robin@obs-besancon.fr

In order to find new constraints on the spheroid density law, we undertook a photometric and astrometric sample survey in various galactic directions. We complemented these data with existing deep photometric star counts in several high and intermediate latitude fields. Most such counts contain large numbers of halo dwarfs, but they cannot be distinguished from thick disc dwarfs by their colours but at faint magnitudes. Since no large optical surveys were available at magnitude fainter than 20, we used heterogeneous data coming from various studies (often of extragalactic aim) in various photometric systems.

The population synthesis model used here permits to perform a global analysis of these heterogeneous data, since observational data can be simulated in each field with the true observational conditions (photometric system, errors and selection effects). The synthetic approach allows also to estimate the biases and expected contaminations by other populations.

In Sect. 2 we describe the model of population synthesis and external constraints on the spheroid population. In Sect. 3 we describe the data sets and the comparison method. In Sect. 4 we discuss the results and their implications for the dark matter halo.

2. The model of population synthesis

We have used a revised version of the Besançon model of population synthesis. Previous versions were described in Bienaymé et al. (1987a; 1987b) and Haywood et al. (1997b).

The model is based on a semi-empirical approach, where physical constraints and current knowledge of the formation and evolution scenario of the Galaxy are used as a first approximation for the population synthesis. The model involves 4 populations (disc, thick disc, halo and bulge) each deserving a specific treatment. The bulge population which is irrelevant for this spheroid analysis will be described elsewhere.

2.1. The disc population

A standard evolution model is used to produce the disc population, based on a set of usual parameters: an initial mass function (IMF), a star formation rate (SFR), a set of evolutionary tracks (see Haywood et al., 1997 and references therein). The disc population is assumed to evolve during 10 Gyr. A set of IMF slopes and SFR's are tentatively assumed and tested against star counts. The tuning of disc parameters against relevant observational data was described in Haywood et al. (1997a; 1997b).

The model fixes the distribution of stars in the space of intrinsic parameters: effective temperature, gravity, absolute magnitude, mass and age. These parameters are converted into colours in various systems through stellar atmosphere models corrected to fit empirical data (Lejeune et al., 1997; Lejeune et al., 1998). While some errors still remain in the resulting colours for some spectral types, the overall agreement is good in the major part of the HR diagram.

Since the Haywood et al. model was based on evolutionary tracks at solar metallicities, inverse blanketing corrections are introduced to give to the disc a metallicity distribution in agree-

ment with Twarog (1980) age/metallicity distribution (mean and dispersion about the mean).

The model returns the present-day distribution of stars as a function of intrinsic parameters in a unit volume column centered at the sun position. Since the evolution model does not account for orbital evolution, stars are redistributed in the reference volume over the z axis. The key for redistributing stars along the z -axis is age: an empirical relation associates z velocity dispersions to ages. Then the Boltzmann equation is used to convert z velocity distributions into z density. The model is dynamically self-consistent in the sense that the potential used in the Boltzmann equation is the one generated by the total mass distribution of stellar populations. The self consistency is established iteratively. We slice the disc populations into seven isothermal populations of different ages, from 0 to 10 Gyr. Each sub-population (except the youngest one, which cannot be considered as relaxed) has its velocity dispersion imposed by the age/velocity dispersion relation. We then deduce the scale height of each sub-population using the Boltzmann equation. The overall scheme is described in Bienaymé et al. (1987a).

Resulting density laws are used to correct the evolution model distribution in and off the plane, then to compute the stellar densities all over the Galaxy.

2.2. The thick disc population

A detailed analysis of the thick disc population from photometric and astrometric star counts has been given elsewhere (Ojha et al., 1994a; Ojha et al., 1994b; Ojha et al., 1996; Robin et al., 1996; Ojha et al., 1999). The kinematics, metallicity, and density law were measured allowing us to constrain the origin for this population. In this series of papers, evidence was given that the majority of thick disc stars should originate from a merging event at the beginning of the life of the thin disc, after the first collapse. One or several satellite galaxies have heated the thin disc, then the gas re-collapsed and reformed a new thin disc (Robin et al., 1996).

In the population synthesis process, the thick disc population is modeled as originating from a single epoch of star formation. We use Bergbusch & Vandenberg (1992) oxygen enhanced evolutionary tracks. No strong constraint exists on the thick disc age until now. We assume an age of 11 Gyr, which is slightly older than the disc and younger than the halo. The initial mass function is modeled by a simple power law with a slope about $\alpha = 1-2$, referring to the notation $\phi(m) \propto m^{-\alpha}$.

The thick disc metallicity can be chosen between -0.4 and -1.5 dex in the simulations. The standard value of -0.7 dex is usually adopted, following in situ spectroscopic determination from Gilmore et al. (1995) and photometric star count determinations (Robin et al., 1996; Buser et al., 1999). The low metallicity tail of the thick disc seems to represent a weak contribution to general star counts (Morrison, 1993b). It was neglected here. An internal metallicity dispersion among the thick disc population is allowed. The standard value for this dispersion is 0.25 dex. No evidence has been found for a significant metallicity gradient in the thick disc population (Robin et al., 1996).

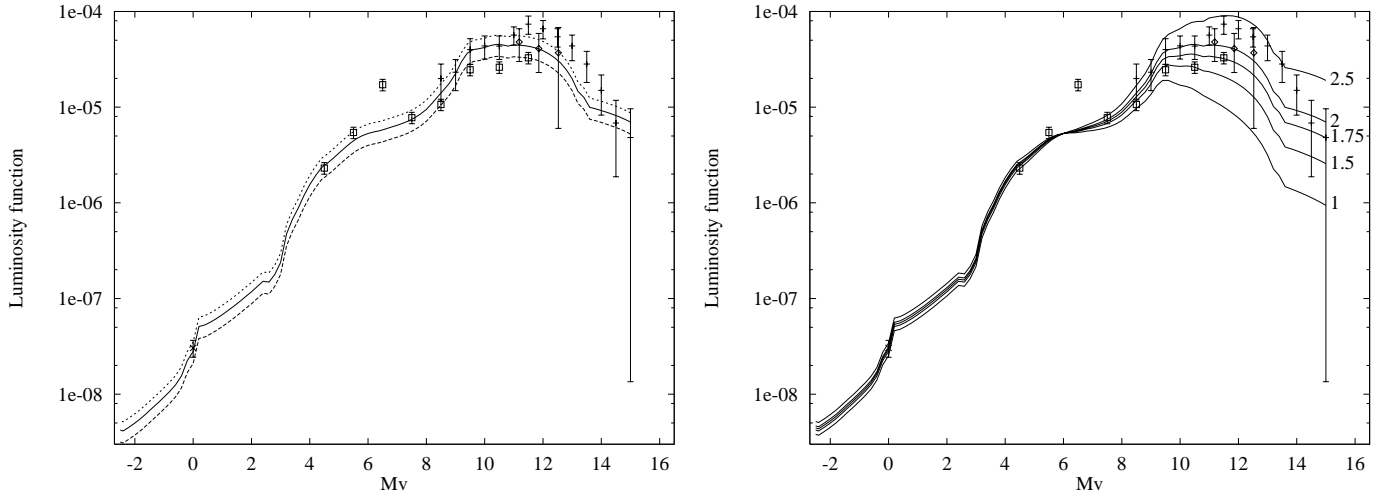


Fig. 1a and b. Luminosity function of the stellar halo. (Gizis & Reid, 1999): diamonds; (Bahcall & Casertano, 1986): squares; (Dahn et al., 1995): plus, (Morrison, 1993a): cross. **a** solid line: modeled luminosity function with an IMF slope (α) of 2.0; the dotted lines give the same luminosity function renormalized by a factor 0.75 or 1.25. **b** luminosity functions as **a** function of IMF slope (as indicated in the graph).

The thick disc density law is assumed to be a truncated exponential: at large distances the law is exponential. At short distances it is a parabola. This formula ensures the continuity and derivability of the density law (contrarily to a true exponential) and eases the computation of the potential. The scale height of the exponential can vary between 600 and 2600 pc. The standard value, 760 pc, has been obtained from star count fitting in various directions (Robin et al., 1996). Nevertheless, it can be shown that star counts when restricted to a small number of galactic directions and a small magnitude range do not give a strong constraint on the scale height, but rather on the parameter: (local density) \times (scale height)². At present there is no accurate determination of the thick disc density in the solar neighbourhood, independently from the scale height. But reasonable values range between 700 to 1200 pc for the scale height and 1 to 4% for the local density relative to the thin disc.

2.3. The spheroid

We assume a homogeneous population of spheroid stars with a short period of star formation. We thus use the Bergbusch & Vandenberg (1992) oxygen enhanced models, assuming an age of roughly 14 Gyr (until more constraints on the age are available), a mean metallicity of -1.7 dex and a dispersion of 0.25 about this value. No galactocentric gradient is assumed. The IMF has to be constrained either from globular clusters (if they are representative of the spheroid population) or from deep star counts. This point is discussed in Sect. 3.

The density of spheroid stars is modeled by a power law:

$$\rho(R, z) = \rho_0 \times \left(R^2 + \frac{z^2}{\epsilon^2}\right)^{n/2}$$

where ρ_0 is the local density, n is the power law index and ϵ is the flattening.

The local density can be constrained by local measurements of high velocity stars, or by remote counts of giants (spectro-

scopically selected) or dwarfs (photometrically selected). The local density cannot be determined independently from the other density parameters with our limited number of data sets. Thus we have used independent constraints from the literature on the local spheroid density.

2.4. The local spheroid density

The local stellar spheroid density, ρ_0 , is bounded by observational data on halo dwarfs and giants. Fig. 1 shows the luminosity function obtained by different authors. We only selected recent results obtained in good conditions from sufficiently large samples. Bahcall & Casertano (1986) and Gizis & Reid (1999) derived their values from high proper motion dwarf samples. Dahn et al. (1995) determined accurate parallaxes for local late-type subdwarfs and deduced the local luminosity function of halo stars in the absolute visual magnitude range 9 to 14. These three results are biased by the kinematic selection. They took the bias correction into account but this correction is model dependent and introduces an unknown uncertainty into the result. We expect that the differences between the three measurements rely upon this correction. On the giant side, Morrison (1993a) used a non kinematically-biased sample of halo giants, selected from their metallicity to estimate the spheroid local density. In Fig. 1a we show the luminosity function from Bergbusch & Vandenberg (1992) for a population of 14 Gyr with a metallicity of -1.75 and an IMF slope α of 2. If we let the local halo density vary from a factor of 0.75 to 1.25 relative to this reference model (dotted lines in Fig. 1a), we get a good agreement with the specified observations given their uncertainties. In the next section we allow the local density to vary within these limits.

3. Data sets and fitting methods

Obtaining good constraints on the spheroid density law requires a good photometric accuracy. This generally depends on using

Table 1. Deep photometric surveys used in our analysis. The magnitude and colour range used to select the halo stars are given.

Reference	Field coordinates	Area (deg ²)	Bands	Magnitude range	Colour range
Our program	North Galactic Pole	0.158	V,I	V=20,24	0,1.6
	l=150°, b=+60°	0.051	V,I	V=20,22	-0.4,1.2
DMS	l=129°, b=-63°	0.144	V,R	V=20,22	0,0.6
	l=248°, b=+47°	0.079	V,R	V=20,22	0,0.6
	l=337°, b=+57°	0.156	V,R	V=20,22	0,0.6
	l=77°, b=+35°	0.153	V,R	V=20,22	0,0.6
	l=52°, b=-39°	0.149	V,R	V=20,22	0,0.6
	l=68°, b=-51°	0.149	V,R	V=20,22	0,0.6
Koo & Kron (1982)	North Galactic Pole	0.097	J,F	J=20,22	-0.4,1.0
	l=111°, b=-46°	0.299	J,F	J=20,22	-0.25,1.0
Reid & Majewski (193)	North Galactic Pole	0.300	V,B	V=20,22	0,0.8
CFRS	l=177.4°, b=-48.3°	0.0105	V,I	I=20,22	-0.4,1.4
	l=205°, b=52°	0.0033	V,I	I=20,22	-0.4,1.4
	l=96.3°, b=59.9°	0.00952	V,I	I=20,22	-0.4,1.4
	l=64°, b=-44.4°	0.0062	V,I	I=20,22	-0.4,1.4

CCD detectors on large telescopes, on fields as wide as possible to cover large samples, and a large range of galactocentric distances. This can be obtained with a number of data sets at various galactic latitudes and longitudes. We have collected such data sets from the literature. Most have been made for extragalactic purposes.

3.1. Available data

The main data characteristics are summarized in Table 1. The photometric systems are close to the Johnson-Cousins system. Spheroid star selection was based on their magnitude and colour (either B-V, V-R, or V-I, depending on the available observations), in order to avoid presence of contamination by other populations. Aiming at model independent results, the model was used essentially to select colour and magnitude ranges and fields where the contamination by thick disc stars remains negligible under any reasonable thick disc hypothesis. For this reason all data brighter than magnitude 20 at intermediate and low latitudes were excluded. A small number of disc white dwarfs is also present in the selection but the proportion is at most a few percent and has no consequence on the result.

Our survey program include at the moment two fields, one towards the north galactic pole, another at intermediate latitude (l=150,b=60). The NGP field is the deepest up to now: it is complete and free from galaxy contamination up to magnitude 24. A full description of these data sets will be given in a forthcoming paper.

The other selected data sets are the six fields of the DMS survey (Hall et al., 1996; Osmer et al., 1998) observed in V and R bands at medium latitude, 4 fields from the Canada-France Redshift survey (CFRS, (Lilly et al., 1995; Le Fevre et al., 1995; Hammer et al., 1995)) dedicated to galaxy counts, two fields from the Koo & Kron investigation for quasars (Koo & Kron, 1982; Koo et al., 1986), another field from Reid & Majewski near the north galactic pole (Reid & Majewski, 1993).

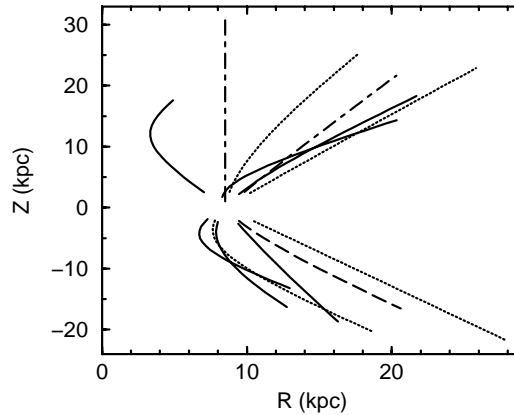


Fig. 2. Line of sight projected on (R,z) plane. The segments limits indicate the distance distribution for 90% of the halo stars. Solid lines indicate the Deep Multicolor Survey fields, dotted lines the Canada-France Redshift Survey fields, long dashed lines the field from Koo & Kron (1982) and the dot-dashed lines the fields from our program, as well as other North Galactic pole fields from Koo et al. (1986) and Reid et al. (1993).

The absolute visual magnitude of halo stars in the selected samples ranges between 3 and 8, except our north galactic pole field which reaches $M_V \sim 11$. All these fields taken together cover a large part of the (R,z) plane, as can be seen in Fig. 2 where the distributions in R and z of 90% of halo stars in each field of view are drawn.

3.2. Analysis method

Population synthesis simulations have been computed in every observed field using photometric errors as close as possible to the true observational errors, generally with photometric errors growing as a function of the magnitude and assumed to be Gaussian. Monte Carlo simulations are done in a solid angle much larger than the data in order to minimize the Poisson noise.

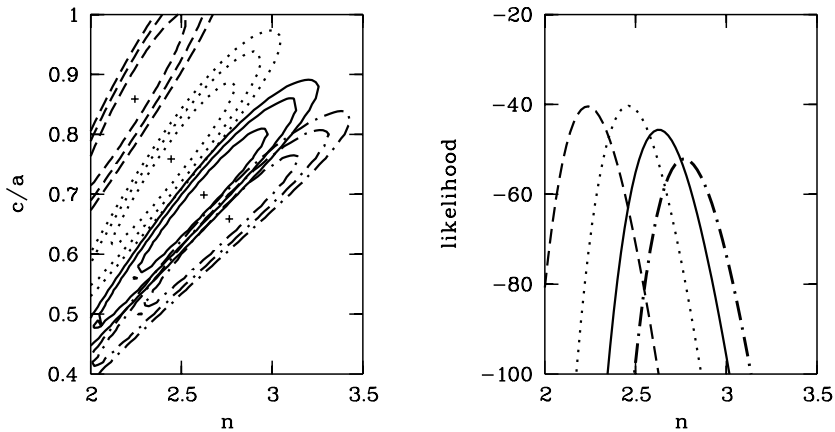


Fig. 3. Likelihood as a function of power law index, flattening and local density: On the left: iso-likelihood contours at 1, 2 and 3 sigmas in the plane (power law index, flattening) of the spheroid population. On the right, likelihood as a function of the power law index, for the best flattening. Lines are coded by the local density. Solid line: standard local density as defined in Sect. 2.4; dotted line: $0.75 \times \rho_0$; dashed: $0.50 \times \rho_0$, dotted-dashed: $1.25 \times \rho_0$

Then we compare the number of stars produced by the model with the observations in the selected region of the plane (magnitude, colour) and we compute the likelihood of the observed data to be a realization of the model (following the method described in Bienaymé et al., 1987a, appendix C). The likelihood has been computed for a set of models, varying the power law index between 2.0 and 3.5, the flattening between 0.3 and 1.0, the local density between 0.5 and 1.25 times the standard value as defined in Sect. 2.4, and the spheroid IMF slope α from 1.0 to 2.2.

The confidence limits of estimated parameters are determined by the likelihood level which can be reached by pure random change of the sample: a series of simulated random samples are produced using the set of model parameters. The rms dispersion of the likelihood about the mean of this series gives an estimate of the likelihood fluctuations due to the random noise. It is then used to compute the confidence limit. Resulting errors are not strictly speaking standard errors, they give only an order of magnitude.

4. Results and discussion

4.1. Constraints on the spheroid density law

Fig. 3 gives the value of the likelihood as a function of the flattening, power law index and local normalization. On the left, iso-likelihood contours are drawn for four values of the local normalization (0.5 , 0.75 , 1.0 and $1.25 \times \rho_0$). On the right, we show the likelihood values as a function of the power law index for the best fit value of the flattening.

Comparing the results of different local normalization we conclude that the choice of the local normalization sensitively displaces the best fit power law index and flattening, but their likelihood are not similar. The best fit model is obtained either with a local density of $0.75 \rho_0$, a power law index of 2.44 and an axis ratio of 0.76, or a local density of $0.5 \rho_0$, a power law index of 2.24 and an axis ratio of 0.86. The values obtained with a standard local density ρ_0 are slightly worse but stay within 1 sigma confidence level. They are a power law index of 2.62 and an axis ratio of 0.70. The best fit local densities $0.5 \rho_0$ and $0.75 \rho_0$ agrees with the Bahcall & Casertano determination of the local luminosity function as seen in Fig. 1, but conflict with Dahn et

al., which favors a local density of $1.25 \rho_0$. However, in the present study the statistics is dominated by stars with absolute magnitudes in the range 3 to 8, a range poorly represented in the Dahn et al. sample. Only deeper counts could give constraints on the fainter part of the luminosity function.

It is worth having a look at the colour distributions as predicted by the best fit model compared with the observational data. Figs. 4 and 5 show the colour distributions observed (dots) and predicted (heavy solid line) by the best fit model ($\epsilon=0.76$, $n=2.44$, $0.75 \rho_0$) in the selected magnitude interval in each tested field. Superimposed we show the distribution of the spheroid population alone as predicted by the model (light solid line). We see here that some photometric systems are not closely matched by the model, as seen by slight shifts between model and data in some cases. But the way we have selected spheroid stars in the blue peak of the distribution cannot introduce a bias even in case of colour shifts.

4.2. Sensitivity to the IMF slope

Whatever the assumed IMF slope in the range 1–2.2, the maximum likelihood is obtained for the same density law parameters. There is a slight likelihood variation related to the choice of the IMF, but it is only due to the deepest magnitude bin towards the pole.

A separate analysis of star counts deeper than 22 towards the pole can help determine precisely the IMF slope. In this magnitude range spheroid stars with absolute magnitude 10–11 contribute substantially to star counts, while their frequency is sensitive to the IMF as can be seen on Fig. 1b. The analysis is slightly different from the determination of the density law. In this range of absolute magnitude the subdwarf sequence turns redwards making the colour index a good luminosity indicator. The V-I distribution is used as an additional constraint. A V-I histogram is built with a bin 0.1 magnitude wide over the range 0 to 3. The density law is adopted from the above analysis, so the free parameters are the halo and thick disc IMF slopes. Since these two populations are quite well separated in the (V,V-I) plane, the two IMF slope estimates are de-correlated. Table 2 gives the resulting slope estimates with their likelihood in the

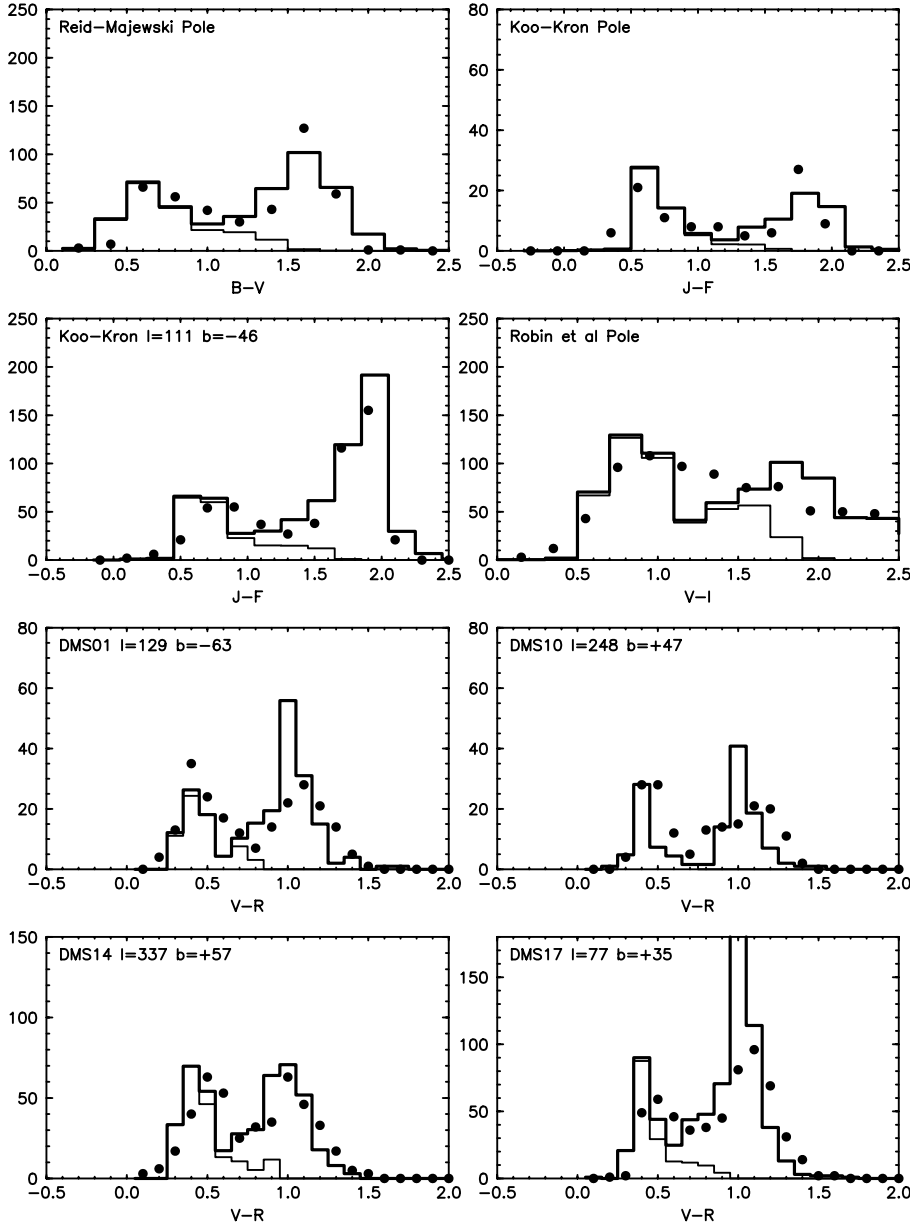


Fig. 4. Colour distributions of selected samples. Contributions of different magnitude interval have been summed up for clarity. Observations in different fields are shown by dots. The ordinates give the true number of observed stars in each colour bin. Heavy solid lines are the predicted number of stars by the model assuming a power law index of 2.44, a flattening of 0.76 and a local density of $0.75 \times \rho_0$ for the spheroid. Thin lines show the contribution of the spheroid alone.

Table 2. IMF slopes of the spheroid and thick disc populations determined by the maximum likelihood technique for four models of spheroid density laws

ρ_0	n	ϵ	α Spheroid	α Thick disc	Likelihood
0.50	2.24	0.86	1.9	1.7	-79.1
0.75	2.44	0.76	1.9	1.7	-58.8
1.00	2.62	0.70	1.9	1.6	-55.9
1.25	2.76	0.66	1.8	1.6	-60.3

magnitude range 22–24 for the different spheroid density laws determined previously.

Spheroid models with a local density $0.75 \rho_0$ and $1.0 \rho_0$ give the maximum likelihood, well in agreement with the previous result. However the model with $0.50 \rho_0$ is noticeably worse.

Eventually, the resulting IMF slopes do not depend significantly on the assumed density laws and the likelihood is well peaked around the maximum indicating a robust determination. We conclude that the IMF of the halo, in the mass range $[0.1, 0.8]$ is:

$$\phi(m) \propto m^{-1.9}$$

while the IMF slope of the thick disc seems to be slightly smaller and similar to the disc's (Haywood, 1994). These values do not account for binarity. Thus the true IMF should slightly steepen. We leave the value uncorrected until more data are available on the binary fraction among low mass spheroid stars.

This result is the first direct measurement of the mass function of field star spheroid with a good statistics, thanks to the wide field of the CCD mosaic. Several previous determinations used kinematically selected samples (see Sect. 2.4 for references) or deep fields. But the latter were limited to narrow fields:

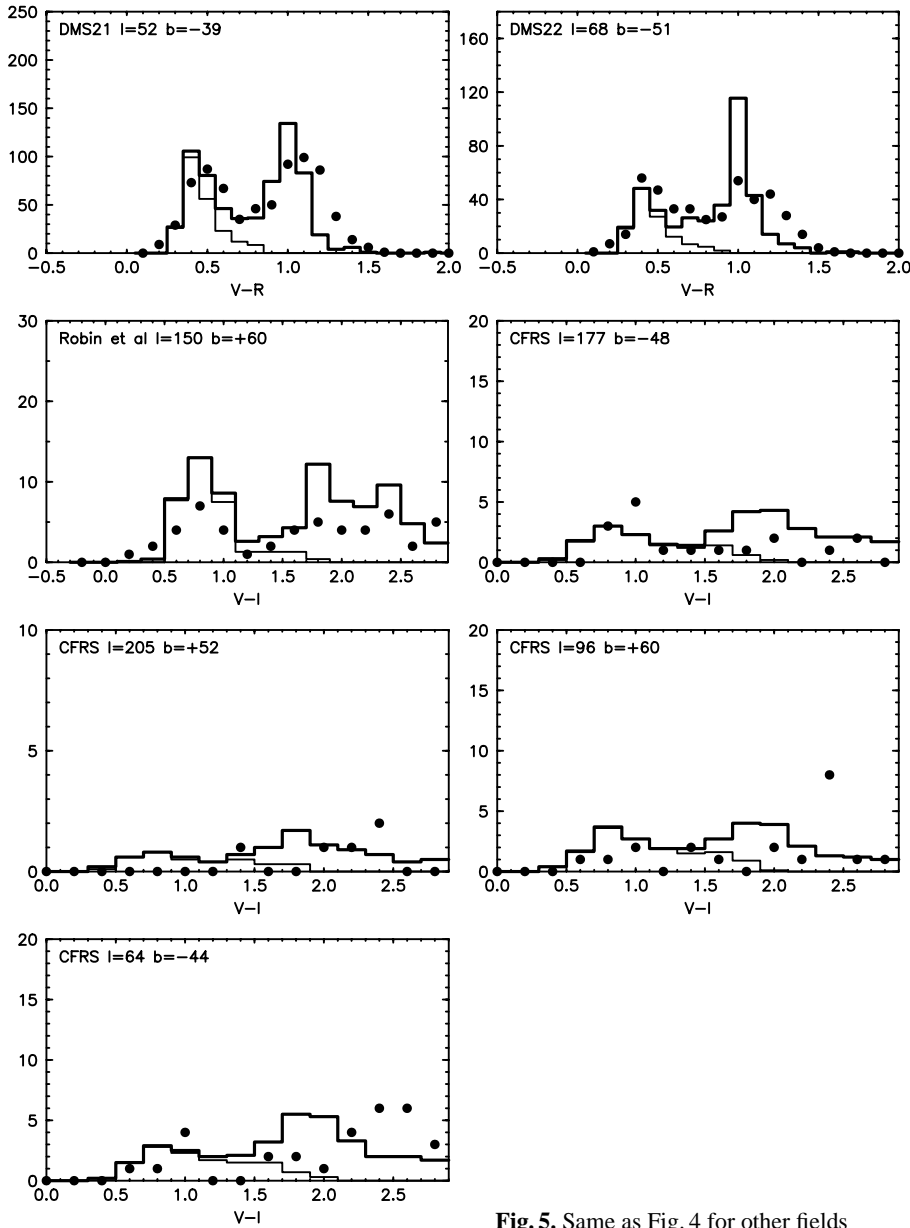


Fig. 5. Same as Fig. 4 for other fields

the first attempt by Richer & Fahlman (1992) lead to a very steep IMF slope of $\alpha = 4.5 \pm 1.2$ which had given hope for a dark matter halo of brown dwarfs. Later results have given shallower slopes but the uncertainties were not significantly decreased.

Gould et al. (1998) analyzed a sample of 166 stars in 53 HST WFPC fields, making difficult the de-correlation between structural parameters of the spheroid and its mass function. They found a luminosity function down by a factor two from the present one and deduced an IMF slope of $\alpha = 0.75$ (in our notation). Their result relies upon the assumption that the spheroid has a mean metallicity of -1.0 , which looks too high considering most direct measurement of its abundances. This high metallicity induces an overestimate of the luminosity at a given colour, hence of the distance, as well as an overestimate of the mass relatively to a smaller assumed metallicity.

4.3. Variations of density law with galactocentric position

If we independently check the results obtained in inner fields and in outer fields, we are able to search for solutions with varying power law index and flattening over the galactic radius. Contrarily to Preston et al. (1991) we find no evidence for varying power law index or flattening. However, a round spheroid is ruled out by the inner field data as well as by fields at low latitudes. Thus our results are compatible with a true power law and a constant flattening all along the tested galactic radius.

When comparing data sets from different sources in close galactic fields, discrepancies appear which are larger than expected on the basis of pure random noise. This may be due either to data incompleteness, or to systematic errors in the photometry (including mismatch of the standard photometric system), or to true inhomogeneities in the spheroid distribution. Cur-

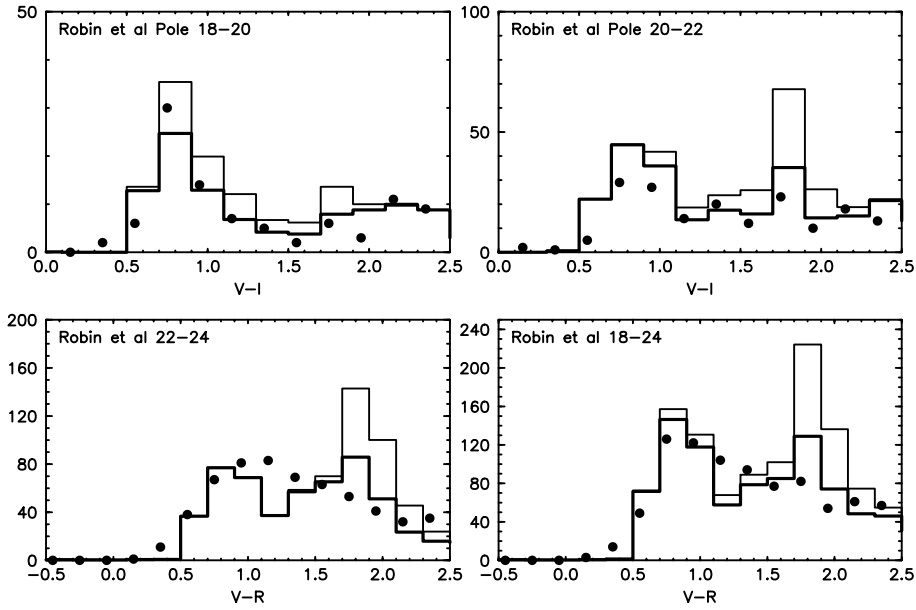


Fig. 6. Colour distributions towards the galactic pole in three magnitude intervals. Dots: observational counts; heavy solid lines: model distribution assuming a standard thick disc, light lines: model assuming a doubled thick disc density. The contamination of the blue peak by the thick disc can reach 30% at magnitudes 18–20 but becomes negligible at fainter magnitudes.

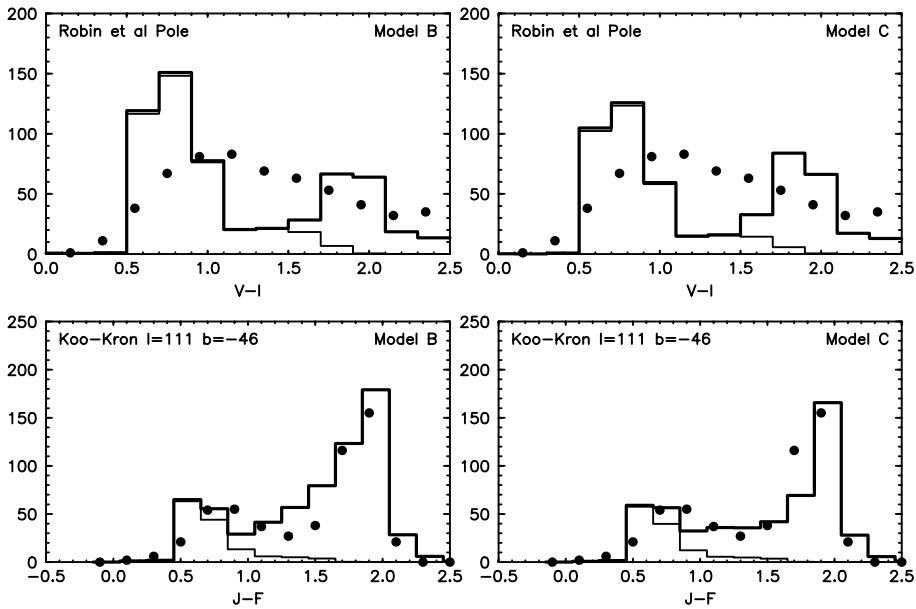


Fig. 7. Observed colour distributions towards the north galactic pole (magnitude range 22–24) and SA68 Koo & Kron data (magnitude range 20–22) compared with model predictions with two thick disc models. On the left side, model B (local density of 3.9% of the thin disc, a scale height of 1150 pc and an IMF slope of $\alpha = 1$), On the right side, model C (local density of 0.5%, scale height 2 kpc, IMF slope 1.75). Thin lines are the contribution of the adjusted spheroid (see text).

rently available data are not sufficient to discriminate between these different causes. Homogeneous wide field surveys will be necessary to clarify these aspects. The scope of the current investigation is for this reason limited to large scale average characteristics.

4.4. Contamination by other populations

The blue peak at these magnitudes may be contaminated by disc white dwarfs or by thick disc main sequence stars. The former are very few compared to the density of the halo. The contamination by disc white dwarfs, as determined by the model, is at most 5% in the magnitude range 22–24.

The contamination from the thick disc has been estimated using our best fit thick disc model as adjusted on medium deep

star counts. The contamination can reach about 30% in the magnitude range 18–20 but becomes negligible at magnitude larger than 20 as seen in Fig. 6. Hence, we do not take into account magnitudes lower than 20 in our study.

Had the thick disc contamination been underestimated, then the contribution assigned to the halo in the blue peak would be too large, resulting in a possible distortion of the density law. In order to evaluate how this would affect our conclusions, we have investigated different thick disc models which could fake the halo contribution to the blue peak. Attempts were limited to realistic thick discs roughly fitting the red peak. We have selected two extreme thick disc parameters for which the contamination to the blue peak becomes significant. A thick disc with a local density of 3.9%, a scale height of 1150 pc and an IMF slope of 1. (referred to as model B). A thick disc with a

scale height of 2 kpc, a local density of 0.5% and an IMF slope of 1.75. (model C). With such thick disc models, the process of adjusting the spheroid density law parameters end up to tiny local density of about 25% of the standard value and very small power law index of the order of 1.5. Surprisingly, the fit is good on star counts up to magnitude 22, showing that a large range of parameters can reproduce a wide set of star counts. However at magnitude 22–24, model B and C are unable to reproduce the counts, as exemplified in Fig. 7, where at the top star counts at the pole in the magnitude range 22–24 are overestimated in the blue peak, and in the range 20–22 (bottom) the fit is still acceptable.

So, the degeneracy between thick disc models and halo parameters holds only if star counts are not deep enough. Keeping reasonable values for the thick disc parameters leads to a small contamination with no risk of underestimation of the halo density. If the thick disc contribution is higher than expected from standard models then we would overestimate the local halo density and power law index, strengthening our conclusion towards a flat spheroid with a small power law index.

5. Conclusions

We have shown that, with the data available up to now, the spheroid star distribution follows a power law with an index smaller than previously thought. It is moderately flattened, as already found by several investigations. The best fit power law index is found 2.44 for a flattening of 0.76. We cannot exclude a spheroid population having a power law as low as 2 and an axis ratio of 0.5 at the 2 sigma level. Assuming a high exponent of 3.5, as suggested by some globular cluster and RR Lyrae data, model predictions deviate significantly from observations in the external parts of the galaxy whatever reasonable flattening is adopted.

The IMF slope of the spheroid is found to be $\alpha = 1.9 \pm 0.2$, value which gives a local density of $1.64 \cdot 10^{-4}$ stars pc^{-3} and a mass density of $4.15 \cdot 10^{-5} M_{\odot} \text{pc}^{-3}$ for the stellar halo, yet this value ignores possible old white dwarfs. With this slope the expected mass density of brown dwarfs in the halo makes a negligible part of the dark matter halo, as already estimated from microlensing surveys.

Recent searches for ancient halo white dwarfs have given a hope to identify the microlensing events with such objects (Ibata et al., 1999; Ibata et al., 2000; Hodgkin et al., 2000). Ibata et al. (2000) conclude that old white dwarfs may constitute a significant fraction of about 10% of the dark matter halo. In the mean time, microlensing experiments have narrowed the range of the estimated halo baryonic fraction to 20 to 50% (Alcock et al., 2000). These two results are well in agreement according to the uncertainties.

So, as star count data progresses in depth and extent, the picture of the spheroid star population that comes out points to characteristics quite compatible with what we know about the distribution of baryonic dark matter if it is made of stellar remnants, suggesting a common dynamical origin. The visible spheroid and its heavy counterpart of dark remnants can make

a significant but not dominant part of the so-called dark matter halo.

References

- Alcock C., Allsman R., Alves D., et al., 2000, *preprint, astro-ph/0001272*
- Alcock C., Allsman R.A., Alves D., et al., 1998, *ApJ* 499, L9
- Alcock C., Allsman R.A., Alves D., et al., 1997, *ApJ* 486, 697
- Aubourg E., Bareyre P., Brehin S., et al., 1993, *Nat* 365, 623
- Bahcall J., 1986, *ARA&A* 24, 577
- Bahcall J., Casertano S., 1986, *ApJ* 308, 347
- Bergbusch P.A., Vandenberg D.A., 1992, *ApJS* 81, 163
- Bienaymé O., Robin A.C., Crézé M., 1987a, *A&A* 180, 94
- Bienaymé O., Robin A.C., Crézé M., 1987b, *A&A* 186, 359
- Buser R., Rong J., Karaali S., 1999, *A&A* 348, 98
- Dahn C.C., Liebert J., Harris H.C., Guetter H.H., 1995, in: Tinney C.G. (ed.), *The bottom of the main sequence and beyond*, pp 239–248, *Proceedings of the ESO Workshop held in Garching, Germany, 10–12 August 1994*. Springer-Verlag
- Gilmore G., Wyse R.F.G., Jones B.J., 1995, *AJ* 109, 1095
- Gizis, J.E., Reid I.N., 1999, *AJ* 117, 508
- Gould A., Flynn C., Bahcall J.N., 1998, *AJ* 503, 798
- Hall P.B., Osmer P.S., Green R.F., Porter A.C., Warren, S.J., 1996, *ApJS* 104, 185+
- Hammer F., Crampton D., Le Fevre O., Lilly, S.J., 1995, *ApJ* 455, 88
- Harris W.E., 1976, *AJ* 81, 1095
- Hawkins M., 1984, *MNRAS* 206, 433
- Haywood M., 1994, *A&A* 282, 444
- Haywood M., Robin A.C., Crézé M., 1997a, *A&A* 320, 428
- Haywood M., Robin A.C., Crézé M., 1997b, *A&A* 320, 440
- Hodgkin S.T., Oppenheimer B.R., Hambly N.C., et al., 2000, *Nat* 403, 57
- Ibata R.A., Irwin M., Bienaymé O., Scholz R., Guibert J., 2000, *ApJ* 532, L41
- Ibata R.A., Richer H.B., Gilliland R.L., Scott D., 1999, *ApJ* 524, L95
- Koo D., Kron R., 1982, *A&A* 105, 107
- Koo D., Kron R., Cudworth K., 1986, *PASP* 98, 285
- Le Fevre O., Crampton D., Lilly S.J., Hammer F., Tresse L., 1995, *ApJ* 455, 60
- Lejeune T., Cuisinier F., Buser R., 1997, *A&AS* 125, 229
- Lejeune T., Cuisinier F., Buser R., 1998, *A&AS* 130, 65
- Lilly S.J., Le Fevre O., Crampton D., Hammer F., Tresse L., 1995, *ApJ* 455, 50
- Morrison H., 1993a, in: *American Astronomical Society Meeting*, Vol. 182, p. 4305
- Morrison H.L., 1993b, *AJ* 105, 539
- Ojha D.K., Bienaymé O., Mohan V., Robin A.C., 1999, *A&A* 351, 945
- Ojha D.K., Bienaymé O., Robin A.C., Crézé M., Mohan V., 1996, *A&A* 311, 456
- Ojha D.K., Bienaymé O., Robin A.C., Mohan V., 1994a, *A&A* 284, 810
- Ojha D.K., Bienaymé O., Robin A.C., Mohan V., 1994b, *A&A* 290, 771
- Osmer P.S., Kenefick J.D., Hall P.B., Green R.F., 1998, *ApJS* 119, 189
- Preston G.W., Shectman S.A., Beers T.C., 1991, *ApJS* 76, 1001
- Reid N., 1993, *MNRAS* 265, 785
- Reid N., Majewski S.R., 1993, *ApJ* 409, 635
- Richer H.B., Fahlman G.G., 1992, *Nat* 358, 383

- Rix H.W., 1996, in: *IAU Symp. 169: Unsolved Problems of the Milky Way*, Vol. 169, pp. 23–29
- Robin A.C., Haywood M., Cr ez e M., Ojha D.K., Bienaym e O., 1996, *A&A* 305, 125
- Sackett P.D., Rix H., Jarvis B.J., Freeman K.C., 1994, *ApJ* 436, 629
- Saha A., 1985, *ApJ* 289, 310
- Sluis A.P.N., Arnold R.A., 1998, *MNRAS* 297, 732
- Sommer-Larsen J., Christensen P.R., 1987, *The Messenger* 47, 13
- Soubiran C., 1993, *A&A* 274, 181
- Twarog B., 1980, *ApJS* 44, 1
- Wetterer C.J., McGraw J.T., 1996, *AJ* 112, 1046
- Zinn R., 1985, *ApJ* 293, 424